

## A Simple Bioreactor-Based Method to Generate Kidney Organoids from Pluripotent Stem Cells

Aneta Przepiorski,<sup>1,4</sup> Veronika Sander,<sup>1,4</sup> Tracy Tran,<sup>2</sup> Jennifer A. Hollywood,<sup>1</sup> Brie Sorrenson,<sup>1</sup> Jen-Hsing Shih,<sup>1</sup> Ernst J. Wolvetang,<sup>3</sup> Andrew P. McMahon,<sup>2</sup> Teresa M. Holm,<sup>1</sup> and Alan J. Davidson<sup>1,\*</sup>

<sup>1</sup>Department of Molecular Medicine & Pathology, University of Auckland, Auckland 1142, New Zealand

<sup>2</sup>Department of Stem Cell Biology and Regenerative Medicine, Keck School of Medicine, University of Southern California, Los Angeles, CA 90089, USA

<sup>3</sup>Australian Institute for Bioengineering and Nanotechnology, University of Queensland, Brisbane, QLD 4072, Australia

<sup>4</sup>Co-first author

\*Correspondence: [a.davidson@auckland.ac.nz](mailto:a.davidson@auckland.ac.nz)

<https://doi.org/10.1016/j.stemcr.2018.06.018>

### SUMMARY

Kidney organoids made from pluripotent stem cells have the potential to revolutionize how kidney development, disease, and injury are studied. Current protocols are technically complex, suffer from poor reproducibility, and have high reagent costs that restrict scalability. To overcome some of these issues, we have established a simple, inexpensive, and robust method to grow kidney organoids in bulk from human induced pluripotent stem cells. Our organoids develop tubular structures by day 8 and show optimal tissue morphology at day 14. A comparison with fetal human kidneys suggests that day-14 organoid tissue most closely resembles late capillary loop stage nephrons. We show that deletion of *HNF1B*, a transcription factor linked to congenital kidney defects, interferes with tubulogenesis, validating our experimental system for studying renal developmental biology. Taken together, our protocol provides a fast, efficient, and cost-effective method for generating large quantities of human fetal kidney tissue, enabling the study of normal and aberrant kidney development.

### INTRODUCTION

The use of stem cell-derived organoids as *in vitro* models to study development and disease has been a major advance in recent years (Lancaster and Knoblich, 2014). Organoids provide an advantage over monolayer cultures due to their complex 3D architecture that better approximates *in vivo* tissues. With regard to the kidney, monolayer cultures have had limited utility for modeling the structure and function of nephrons (the tubular units responsible for filtering the blood and maintaining salt and fluid homeostasis). This is not surprising, given that nephrons are subdivided into functionally distinct portions that act in series to generate the urine. Specifically, the renal corpuscle, containing interdigitating podocytes wrapped around a capillary tuft, generates a plasma ultrafiltrate that travels via the proximal tubule, descending and ascending limbs of the loop of Henle, and more distal segments (distal convoluted tubule, connecting tubule) to the collecting duct (McMahon, 2016).

Early protocols for converting pluripotent stem cells into renal cells attempted to mimic the developmental signals governing early kidney formation from the intermediate mesoderm. A cocktail of secreted factors including low doses (3–5  $\mu$ M) of the Wnt agonist CHIR99021 (CHIR) were found to induce intermediate mesoderm-like cells (Mae et al., 2013; Lam et al., 2014). However, the major breakthrough in the field was the discovery that higher concentrations of CHIR (8  $\mu$ M) followed by fibroblast growth factor 9 (FGF9) (Barak et al., 2012; Takasato et al., 2014), a growth factor required for nephron progenitor

growth *in vivo*, was sufficient to induce kidney organoids with a global transcriptional profile similar to first-trimester fetal kidneys (Takasato et al., 2015). Subsequent methodologies showed that FGF9 can be substituted for B27, a serum-free supplement used to maintain neurons in cell culture (Freedman et al., 2015). In addition, more complex combinations of activin A, bone morphogenetic proteins, and FGF9 have been used to achieve kidney organoid formation (Morizane et al., 2015; Taguchi et al., 2014). How these factors induce a kidney program in pluripotent stem cells remains poorly understood, although it has been suggested that high levels of CHIR may mimic the Wnt signals that induce the posterior mesoderm where nephron progenitors arise (Takasato and Little, 2016). A major drawback of the current protocols is the high cost of the reagents, with FGF9 and B27 being prohibitively expensive, thus severely limiting the large-scale culture of kidney organoids.

Despite commonalities in the factors used to induce kidney organoid formation, the existing protocols differ in their technical details and are overall quite complex. For instance, the method of Taguchi et al. (2014) requires co-culture with spinal cord explants (as a source of Wnt), that of Takasato et al. (2015) involves repeated CHIR treatments, cell dissociation, and then re-aggregation on transwell filters, while Freedman et al. (2015) generate epiblast “spheroids” that are cultured in a Matrigel sandwich. How reproducible these protocols are between different pluripotent stem cell lines has been highlighted as a concern (Morizane and Bonventre, 2017a; Cruz et al., 2017) and as patient-derived and gene-edited induced

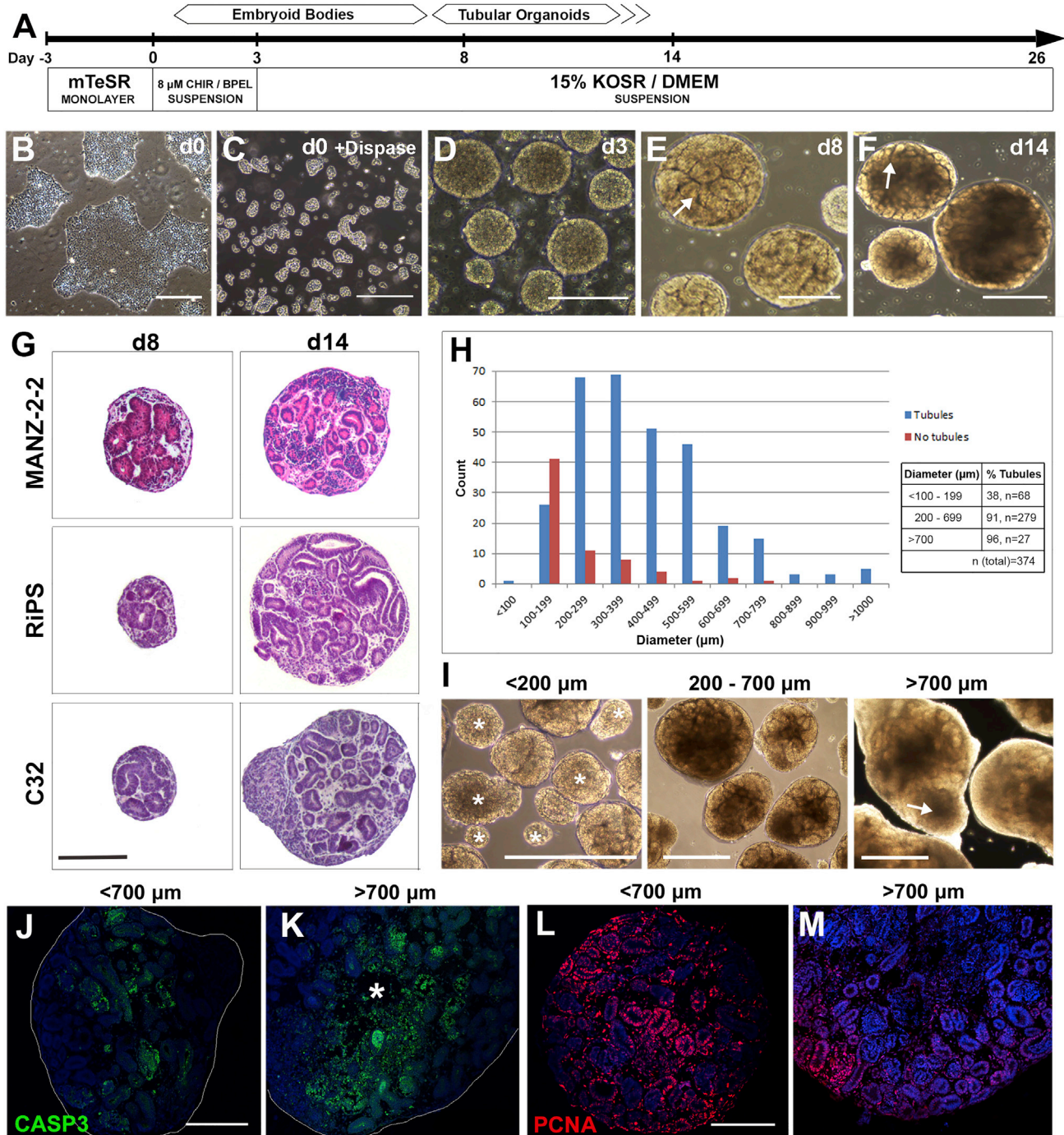


**Figure 1. Derivation of Kidney Organoids from Three iPSC Lines**

- (A) Overview of the protocol.  
 (B) Starting iPSC colonies.  
 (C) iPSC colonies in suspension after dispase digest (mean size  $105 \pm 37 \mu\text{m}$ ,  $n = 142$ ).  
 (D) Embryoid bodies.  
 (E and F) Kidney organoids at day 8 (d8) and day 14; formation of tubules is visible on the surface (arrows).  
 (G) H&E-stained organoid sections derived from three independent iPSC lines at days 8 and 14,  $n \geq 3$  sections.  
 (H) Relationship between organoid size, number, and presence of tubules at day 14 ( $n = 374$  organoids in a single representative assay).

(legend continued on next page)



pluripotent stem cell (iPSC) lines from diverse backgrounds continue to be produced, a protocol with universal utility is highly desirable.

To overcome some of these issues, we have developed a strategy for generating kidney organoids from iPSCs that is simple, robust, and cost-effective, and allows large-scale organoid production. Our method involves the formation of embryoid bodies (EBs) in the presence of CHIR, followed by culture in medium supplemented with “KnockOut Serum Replacement” (KOSR) as a substitute for FGF9. Importantly, this approach is inexpensive and highly efficient, allowing kidney organoids to be grown in spinner flasks. The resulting organoids develop nephrons containing podocytes, proximal and distal tubule segments, presumptive collecting ducts, endothelial cells, and interstitial cells that are comparable with the tissues reported using other methods. Comparison with human fetal kidneys reveals that our organoid nephrons most closely correspond to the late capillary loop stage of differentiation. Prolonged culture of our kidney organoids is associated with an expansion in interstitial cells and their conversion into pro-fibrotic myofibroblasts, suggesting that this may be a new model to study renal fibrosis. We further show that our protocol can robustly generate organoids of equivalent quality from three different iPSC lines without a need for line-specific optimization. Finally, we show that disruption of *HNF1B*, a gene implicated in congenital kidney malformations, results in agenesis of kidney tubules, highlighting the value of our method for the study of human kidney development and birth defects.

## RESULTS

### A Simple, Cost-Effective Method to Generate Kidney Organoids

We developed a protocol to differentiate human iPSCs into kidney organoids in large numbers via an EB formation step using CHIR, KOSR, and simple spinner-flask bioreactors (Figure 1A). Specifically, the initial setup of the assay involves growing iPSC colonies in a monolayer to 40%–50% confluence (Figure 1B). On day 0, the colonies are enzymatically detached and mechanically fragmented into ~100- $\mu\text{m}$  sized pieces by pipetting (Figure 1C), and transferred into ultra-low attachment 6-well plates for suspension culture. A 3-day treatment window with 8  $\mu\text{M}$

CHIR in BPEL (BSA poly(vinyl alcohol) essential lipids) medium (Ng et al., 2008; Orlova et al., 2014) was found to be sufficient to induce aggregation of the colony fragments into spherical EBs (Figure 1D). We discovered that culturing the CHIR-induced EBs in DMEM with 15% KOSR (“Stage II” medium) from day 3 onward supported tubule formation that was visible under bright-field microscopy by day 8 (Figure 1E). Gene expression analysis over the course of days 1–8 suggests that our approach recapitulates the developmental program of mesoderm formation and nephrogenesis, with downregulation of mesodermal genes by day 4 that coincides with a rise in renal progenitor markers (Figure S1A). As spinner-flask bioreactors have been found to improve oxygen and nutrient perfusion (Pagliuca et al., 2014; Martin and Vermette, 2005), we transferred the organoids into 125-mL spinner flasks at day 8. We found that spinner-flask culture of kidney organoids allows concurrent growth and maturation of hundreds of organoids containing tubular kidney tissue by day 14 (Figure 1F). From a single 10-cm plate of iPSCs we can generate approximately 1,000 organoids (Figure S1B). This approach is cost-prohibitive using other existing methods, but is feasible in our method due to the low reagent cost of the KOSR/DMEM medium.

Histological analysis of day-8 and day-14 kidney organoids confirmed the presence of tubular epithelia, interstitial cells, and regions resembling primitive glomeruli (Figures 1G and S2A). Comparable results were obtained when the protocol was applied to three independently reprogrammed iPSC lines: MANZ-2-2, RiPS, and CRL1502-C32 (herein referred to as C32), and in multiple batches from a single line (Figure S2B), although C32 had more of a propensity to form non-renal outgrowths (Figure 1G). In terms of efficiency (number of organoids that contain nephron-like structures), we found no major differences between the iPSC lines with kidney organoids comprising 80%–90% of the total number of organoids at day 8 ( $n = 744/787$  for RiPS;  $n = 469/553$  for MANZ-2-2;  $n = 848/989$  for C32;  $\geq 3$  independent assays per line). Specimens that did not contain tubular structures were clearly distinguishable using bright-field microscopy, and immunohistological analysis confirmed a lack of renal structures and a large proportion of vimentin<sup>+</sup> mesenchymal cells (Figure S3). We also found that the average diameter of the organoids gradually increased from day 8 to day 26, consistent with growth occurring during this time frame (Figure S1C).

(I) Bright-field images of organoids in the <200, 200–700, and >700  $\mu\text{m}$  size ranges. The small non-tubular specimens are marked with asterisks; a non-tubular outgrowth is indicated by the arrow.

(J–M) Immunofluorescent staining of sections from “small” (<700  $\mu\text{m}$ ) and “large” (>700  $\mu\text{m}$ ) organoids showing apoptotic cells stained for activated CASP3 (green) and the proliferation marker PCNA (red). Asterisk in (K) marks a central region with reduced cellularity.  $n \geq 3$  sections per antibody. Nuclear counterstain: DAPI.

Scale bars, 200  $\mu\text{m}$  (D, E, G, and J–M), 400  $\mu\text{m}$  (C and F), and 500  $\mu\text{m}$  (B and I).



We next analyzed a representative organoid assay to determine whether there was a correlation between organoid diameter and the presence of tubules at day 14. We found tubules in only ~40% of the organoids with diameters <200  $\mu\text{m}$  but in ~90% of the organoids with diameters  $\geq 200 \mu\text{m}$  (Figures 1H and 1I, single representative assay shown). As our protocol involves growing the tissue in suspension, we were able to introduce a simple size filtration step using a 200- $\mu\text{m}$  strainer to eliminate these smaller organoids that were enriched for non-renal tissue. In the organoids remaining after this size selection, tubule formation was highly efficient (96%), although this subset contains organoids that have diameters >700  $\mu\text{m}$  (Figures 1I and S1C), possibly due to insufficient fragmentation of the iPSC colonies at day 0 and/or EB fusion. Given that the diffusion of oxygen and nutrients becomes limiting as organoid diameter increases (Hubert et al., 2016; Winkle et al., 2012), we examined whether apoptosis was occurring in day-14 organoids in the 200–700  $\mu\text{m}$  and >700  $\mu\text{m}$  size ranges using immunostaining for activated caspase-3 (CASP3) on day-14 organoid sections. While few CASP3<sup>+</sup> cells were found scattered throughout the tissue and around clusters of presumptive podocytes in <700- $\mu\text{m}$  organoids (Figure 1J), >700- $\mu\text{m}$  organoids exhibited a notable loss of cellularity in their cores (asterisk in Figure 1K) and displayed qualitatively more CASP3<sup>+</sup> cells throughout the tissue. As a further assessment of organoid viability, we performed immunostaining for the proliferation marker PCNA (proliferating cell nuclear antigen). Proliferating cells were widespread throughout <700- $\mu\text{m}$  organoids (Figure 1L) but in >700- $\mu\text{m}$  organoids, cell division was largely restricted to peripheral regions (Figure 1M). Together, these observations indicate that large organoids (>700  $\mu\text{m}$ ) are associated with central apoptosis and reduced proliferation, suggesting that they may not be as viable as smaller organoids. Based on this, we incorporated an additional size filtration step using a 500- $\mu\text{m}$  strainer to remove these large organoids.

### Kidney Organoids Are Composed of Immature Nephrons

To evaluate nephron differentiation in day-14 organoids we surveyed a range of markers by immunostaining. We identified MEIS1/2/3<sup>+</sup> interstitial cells and PECAM1/CD31<sup>+</sup> endothelial cells that were scattered throughout the tissue, although in variable numbers (Figures 2A and 2B). The endothelial cells were often found in close proximity to primitive glomeruli-like structures, which contained cells that stained for the podocyte marker Wilms' tumor suppressor 1 (WT1; Figure 2B). Electron microscopy revealed that the podocytes display an immature appearance at day 14 with areas of broad cell-cell contacts. Culture of the organoids to day 26 resulted in more elaborate cell

cell junctions, resembling the early stages of foot process formation (Figures 2C–2F).

In addition to podocytes (which also labeled with NPHS1/Nephrin; Figure 3A), day-14 organoids contained kidney tubules that were subdivided into proximal segments that stain for *Lotus tetragonolobus* lectin (LTL) and distal portions that label with cadherin-1 (CDH1; Figure 3A). There was little overlap of LTL and CDH1 except in short stretches at their junction in rare tubules (arrows in Figure 3A and Video S1 of a serial z stack through a whole-mount stained organoid). LTL staining was strong apically in proximal tubule cells but also weakly marked the basolateral surface. As mature proximal tubules are subdivided into S1–S3 domains, we co-stained the organoids for LTL and LRP2/megalin, the latter of which is predominantly expressed in the S1 and S2 segments in mature nephrons (Christensen et al., 1995). We found that the staining patterns of LTL and LRP2 fully overlap, indicating that the proximal tubules have not undergone any further subsegmentation at this stage (Figure 3B). Consistent with this relatively immature state of the proximal tubule, apical microvilli were not readily detected at day 14 and are rudimentary at day 26 by electron microscopy (Figures 3C and 3C'). Despite these immature features, incubation of the organoids with 10-kDa Rhodamine-labeled dextran for 48 hr resulted in the specific uptake of the dextran into LTL<sup>+</sup> tubules, indicating that the absorptive function of the proximal tubule is acquired early in nephrogenesis (Figure 3D).

Next, we explored the identity of the distal portion of the nephron. Morphologically, there was no indication of descending or ascending thin limbs, which form part of the loop of Henle and are positioned between the proximal tubule and the thick ascending limb segment. In agreement with this observation, we found that LTL<sup>+</sup> cells abut a short segment that stains for SLC12A1 and uromodulin (UMOD), markers expressed by the thick ascending limb (Figures 3E and 3F; arrows). While we were unable to detect the distal convoluted tubule marker SLC12A3 at this stage, we did find positive staining for GATA3 and calbindin-1 (CALB1), which label the distal convoluted tubule, connecting tubule, and cortical collecting duct in mature adult nephrons (Figures 3G and 3H; Kumar et al., 1994, Labastie et al., 1995, Kirk et al., 2010, Mantilla et al., 2017, Lindstrom et al., 2018a). Interestingly, CALB1 was found to label an internal subdomain of the GATA3<sup>+</sup> epithelium (Figure 3H), possibly reflecting the collecting duct based on recent marker analyses in fetal human kidneys (Lindstrom et al., 2018a). At the ultrastructural level, presumptive collecting duct and/or distal tubule cells (identified based on their columnar shape and nuclear morphology) display large lumens, well-defined cell junctional complexes, few apical microvilli, and prominent vesicular bodies by day 26 (Figures 3I and 3I').

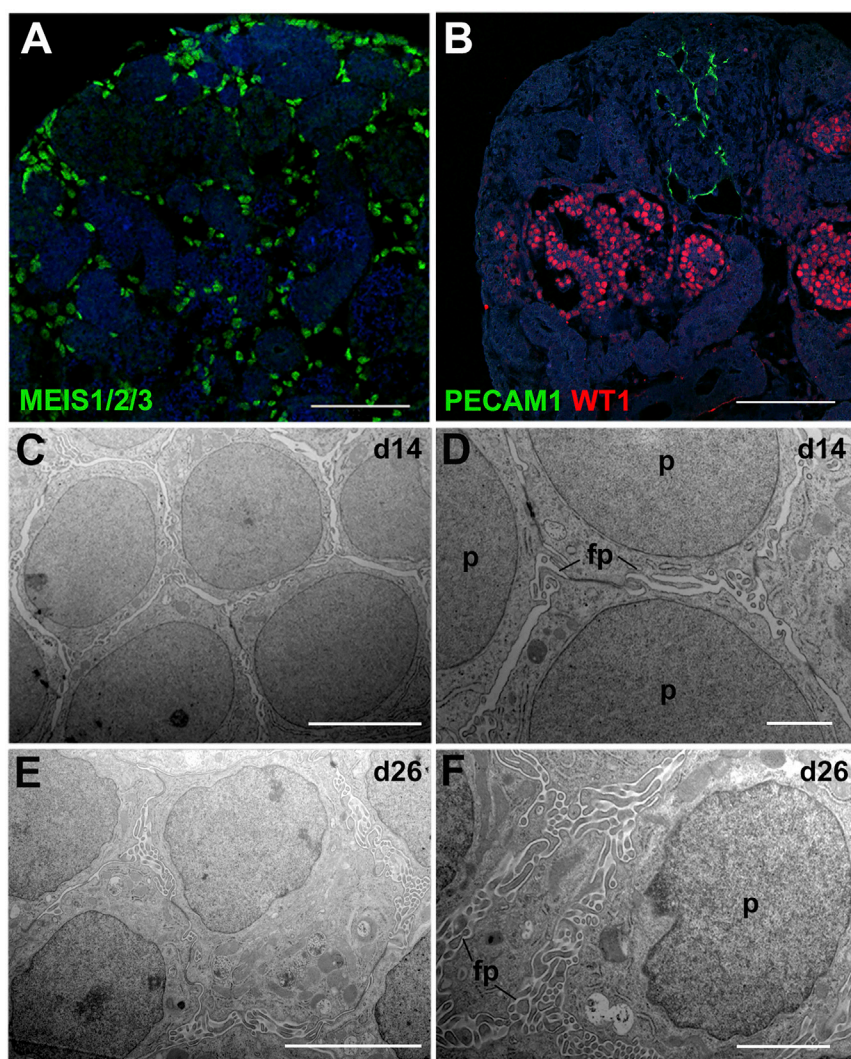


**Figure 2. Stromal and Glomerular Marker Analysis in Kidney Organoids**

(A and B) Immunostaining of paraffin sections of day-14 organoids showing (A) MEIS1/2/3<sup>+</sup> interstitial cells (green) and (B) WT1<sup>+</sup> podocytes (red) and PECAM1<sup>+</sup> endothelial cells (green) ( $n \geq 3$  sections per antibody combination). (C–F) Transmission electron micrograph (TEM) images of podocytes (p) with primitive foot processes (fp) at day 14 (C and D) and more developed foot processes at day 26 (E and F;  $n \geq 3$  images). Nuclear counterstain: DAPI (A and B). Scale bars, 2  $\mu\text{m}$  (D and F), 5  $\mu\text{m}$  (C and E), and 100  $\mu\text{m}$  (A and B).

To further assess the differentiation state of day-14 organoid nephrons we examined PAX2, as this transcription factor is downregulated following terminal differentiation of renal epithelial cells (Dressler and Woolf, 1999). We found low levels of PAX2 in the proximal tubules but slightly higher levels in the distal nephron/presumptive collecting duct, consistent with an immature level of differentiation (Figure 3J). Collectively these data show that day-14 kidney organoids, in comparison with mature human nephrons (Figure 3K), are composed of immature nephrons made up of a primitive glomerulus, an LTL<sup>+</sup>/LRP2<sup>+</sup> proximal tubule segment most likely attached to an SLC12A1<sup>+</sup> thick ascending limb segment, and a distal portion most likely comprising one or more nascent distal tubule segments attached to a GATA3<sup>+</sup>/CALB1<sup>+</sup> collecting duct (Figure 3L). Organoids derived from three independent iPSC lines displayed similar marker expression (Figure S4).

### Extended Organoid Culture Leads to Altered Nephron Differentiation

As day-14 organoids are immature, we were interested to find out whether longer culture times would improve differentiation. It has been suggested that co-labeling of LTL and CDH1 is a sign of proximal tubule maturity (Takasato et al., 2015). Similar to data reported for other protocols, we also observed tubules that were double positive for LTL and CDH1 in day-26 organoids (Morizane and Bonventre, 2017a; Brown et al., 2015). In a subset of these, the double-labeled portions were part of large, abnormally branched structures (arrow in Figure 4A). To help interpret these results, we investigated the staining pattern of LTL and CDH1 in normal human fetal kidneys at weeks 15–16 of gestation. LTL staining was first apparent in proximal tubules at the early capillary loop stage and became strongly apical (but not basolateral) in proximal tubules

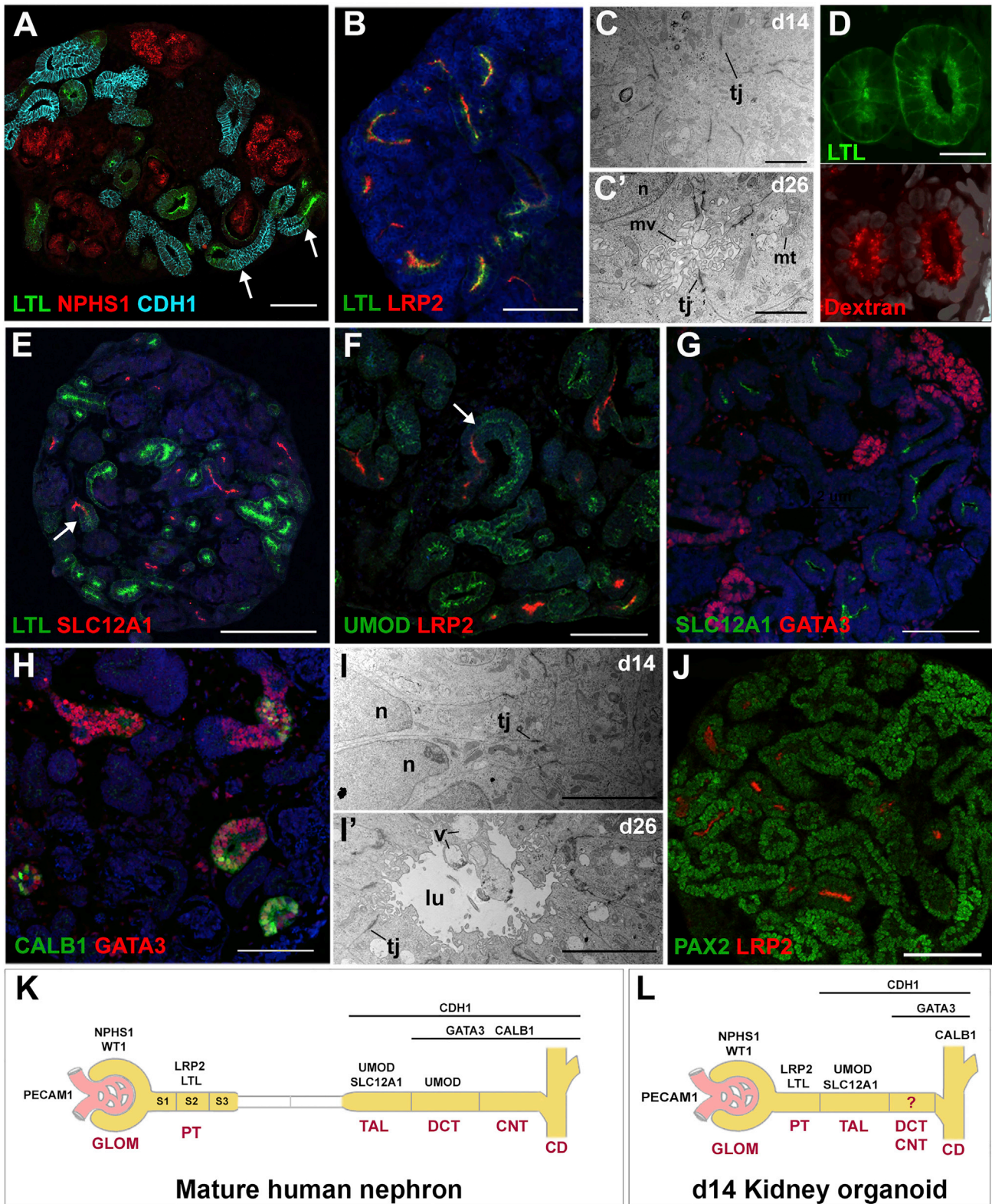


**Figure 3. Tubular Marker Analysis in Kidney Organoids**

(A) Paraffin sections of day-14 organoids showing (A) LTL<sup>+</sup> proximal tubules (green), CDH1<sup>+</sup> distal tubules and collecting ducts (light blue), and NPHS<sup>+</sup> podocytes (red).

(legend continued on next page)



that were identified by co-labeling with cubilin (Figures 4B and 4C). Importantly, CDH1 was only found in the distal portions of the developing nephrons. In more mature fetal nephrons, co-labeling of LTL and CDH1 was detected in some tubules (both apically and basolaterally) but only in the descending limb of the developing loop of Henle in the medulla (Figure S5A). SLC12A3 could not be detected in either early or late capillary loop stage nephrons, consistent with this marker appearing late in human nephrogenesis (Lindstrom et al., 2018a; 2018b).

To determine whether LTL and CDH1 co-label fully mature proximal tubules, we analyzed human adult kidney tissue. Similar to the fetal findings, LTL and CDH1 staining do not overlap in the cortex or in the loops of Henle but occasional co-labeling is seen in collecting ducts in the inner stripe of the medulla (Figures 4D and S5B). Based on these observations, we conclude that endogenous fetal and adult human proximal tubules do not co-label with LTL and CDH1, thus the mixed (LTL<sup>+</sup>/CDH1<sup>+</sup>) identities seen in the organoids may reflect abnormal changes in the tubules following extended culture. Alternatively, this may indicate their conversion to a descending limb-like identity. To further explore whether these changes are associated with altered differentiation, we measured the expression of the lineage markers *NPHS1*, *PECAM1*, *LRP2*, *SLC12A1*, *CALB1*, and *GATA3* in whole organoids at day 8, day 14, and day 26 by qPCR. While most of these markers increased from day 8 to day 14 there was a significant downregulation of *NPHS1* (podocytes), *LRP2* (proximal tubule), *SLC12A1* (thick ascending limb), and *CALB1* (collecting duct) between days 14 and 26 (Figure 4E). A similar downregulation of these markers was observed in the APEL medium used by Takasato et al. (2015), suggesting that this was not due to our DMEM/KOSR medium (data not shown). To assess whether the reduction in nephron marker expression at day 26 was associated with compromised tubule function, we performed the fluorescent dextran uptake assay on

day-26 organoids and found that proximal tubule absorption was significantly impaired (Figure S6). Taken together, our findings suggest that LTL<sup>+</sup>/CDH1<sup>+</sup> tubules are unlikely to represent mature proximal tubules and that longer organoid culture beyond day 14 results in a downregulation of marker gene expression, loss of proximal tubule absorptive functionality, and the formation of potentially abnormal LTL<sup>+</sup>/CDH1<sup>+</sup> tubules. Based on the comparison with human fetal kidneys, our day-14 organoid nephrons approximate late capillary loop stage nephrons.

### Organoids at Day 26 Show Fibrosis and Interstitial Cell Expansion

From a histological comparison of day-14 and day-26 organoids, we noticed that the stromal compartment was expanded at day 26 and accompanied by an accumulation of extracellular matrix. As this is reminiscent of fibrosis, we performed Masson's trichrome staining on day-14 and day-26 organoids and found that while day-14 organoids show little staining, day-26 organoids display collagen staining around the tubules (Figure 5A). Immunostaining for  $\alpha$ -smooth muscle actin (ACTA2), which labels myofibroblasts responsible for the production of fibrotic tissue, revealed a capsule-like layer around day-14 organoids but no internal labeling. In contrast, day-26 organoids display both capsule-like and interstitial staining, suggesting that between day 14 and day 26 myofibroblasts arise and deposit a collagen-rich extracellular matrix (Figure 5B). We next compared the MEIS1/2/3<sup>+</sup> renal interstitial cells at days 14 and 26 and found that this population was qualitatively expanded at day 26 (Figure 5C). We also noted that between days 14 and 26 there was a change in the pattern of proliferation, with day-14 organoids showing PCNA<sup>+</sup> cells in both nephrons and interstitial cells (Figure 1L) whereas in day-26 organoids only rare tubular cells are PCNA<sup>+</sup> (Figure 5D). Co-labeling of ACTA2 with MEIS1/2/3 and PCNA in day-26 organoids revealed extensive

- 
- (B) Co-labeling of LTL (green) and LRP2 (red) in proximal tubules.  
(C and C') TEM images showing proximal tubules with mitochondria and tight junctional complexes at day 14 (C). Rudimentary microvilli are detected at day 26 (C').  
(D) Uptake of 10-kDa dextran-rhodamine (red) into LTL<sup>+</sup> proximal tubules at day 14 (green; n = 8, representative of three independent differentiations).  
(E) LTL<sup>+</sup> proximal tubules (green) and SLC12A1<sup>+</sup> thick ascending limb segments (red).  
(F) LRP<sup>+</sup> proximal tubules (red) and UMOD<sup>+</sup> thick ascending limb segments (green).  
(G) SLC12A1<sup>+</sup> thick ascending limb segments (green) and GATA3<sup>+</sup> tubules/ducts (red).  
(H) Co-staining of GATA3 (red) and CALB1 (green) in the collecting duct.  
(I and I') TEM images of presumptive collecting ducts at day 14 (I) and day 26 (I') showing large lumen and tight junctions.  
(J) Co-staining of PAX2 and LRP2.  
(K and L) Schematic representations of the segmentation patterns of mature human nephrons (K) and day-14 kidney organoids (L). Arrows indicate junctions between segments. Nuclear counterstain: DAPI (blue in B and E–H, gray in D). lu, lumen; mt, mitochondria; mv, microvilli; n, nucleus; tj, tight junction; v, vesicle. n  $\geq$  3 sections per antibody combination or TEM images. Scale bars, 2  $\mu$ m (C and C'), 20  $\mu$ m (D), 5  $\mu$ m (I and I'), 100  $\mu$ m (A, F–H, and J), and 200  $\mu$ m (B and E).

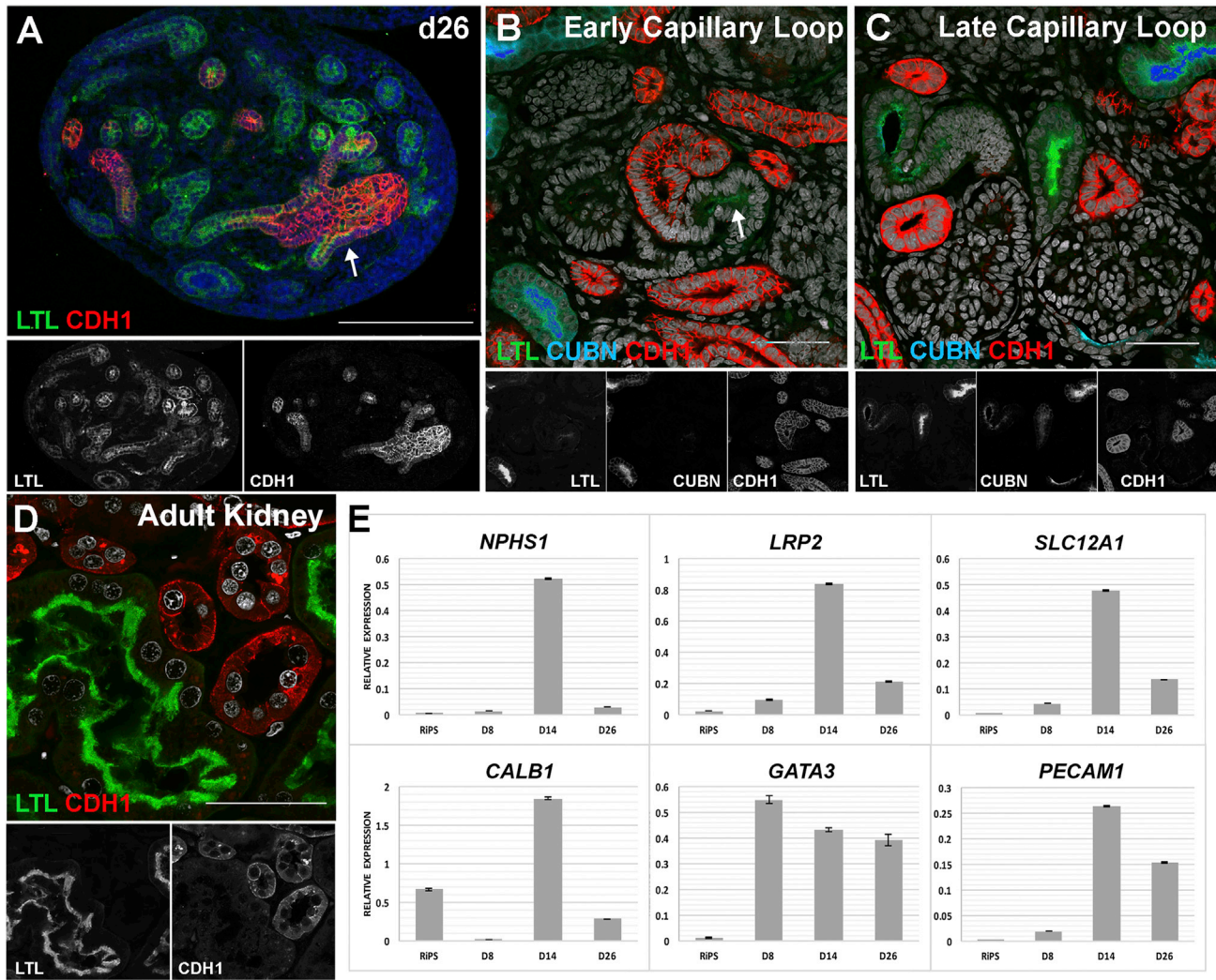


**Figure 4. Marker Analysis in Day-26 Organoids and Human Kidney Tissue**

(A) Paraffin section of day-26 kidney organoid showing partial overlap of LTL and CDH1 in tubules. Arrow points to abnormally branched structures.

(B and C) Cryosections of human fetal kidney (15–16 weeks gestation) showing LTL<sup>+</sup> (green; arrow) and CUBULIN<sup>+</sup> (CUBN; blue) proximal tubules and CDH1 (red) in distal tubules in early (B) and late capillary loop (C) stage nephrons.

(D) Paraffin section of an adult human kidney showing non-overlapping staining of LTL (green) and CDH1 (red).  $n \geq 3$  sections per antibody combination.

(E) qPCR analysis for selected markers in the RiPS line and kidney organoids at days 8, 14, and 26. Data are presented as means  $\pm$  SD from technical triplicates. Nuclear counterstain: DAPI (blue in A, white in B–D).

Scale bars, 50  $\mu$ m (B–D) and 200  $\mu$ m (A).

proliferation of the interstitial cells and a transition to a myofibroblast-like phenotype (Figures 5E and 5F). In summary, these results suggest that organoid viability is optimal around day 14, when the tissue has small amounts of MEIS1/2/3<sup>+</sup> interstitial cells and no evidence of fibrosis. After day 14, nephron components of the organoid exhibit reduced proliferation while the interstitium continues to expand with some cells converting to an ACTA2<sup>+</sup> myofibroblast-like (presumptive pro-fibrotic) state.

### HNF1B Knockout Organoids as a Model of Congenital Kidney Defects

To test the utility of our kidney organoids to study human nephrogenesis, we targeted the *HNF1B* transcription factor gene, which has been shown to play essential roles in tubulogenesis and is implicated in congenital anomalies of the kidney and urinary tract (Nakayama et al., 2010; Naylor et al., 2013; Heliot et al., 2013; Massa et al., 2013; Clissold et al., 2015). Using CRISPR/Cas9 gene editing in MANZ-2-2

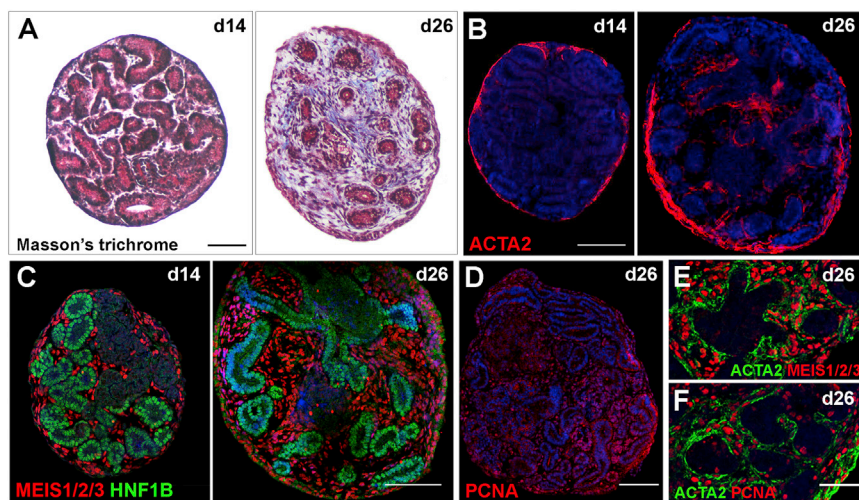


**Figure 5. Analysis of Fibrosis and Interstitial Cells in Day-26 Organoids**

(A) Paraffin sections of day-14 and day-26 organoids stained with Masson's trichrome showing collagen deposition at day 26 (blue).  $n \geq 3$  sections per time point.

(B–F) Immunostainings of day-14 and day-26 organoids showing: (B)  $\alpha$ -smooth muscle actin (ACTA2)-labeled myofibroblasts (red); (C) MEIS1/2/3<sup>+</sup> interstitial cells (red) and HNF1B<sup>+</sup> tubules/ducts (green); (D) PCNA<sup>+</sup> (proliferating) cells (red); (E and F) Co-labeling of the myofibroblast marker ACTA2 (green) with MEIS1/2/3 (red) in (E) and PCNA (red) in (F).  $n \geq 3$  sections per antibody combination. Nuclear counterstain: DAPI.

Scale bars, 50  $\mu\text{m}$  (F; also applies to E) and 100  $\mu\text{m}$  (A–D).

iPSCs, we generated three independently derived iPSC lines with biallelic deletions in exon 2 of the *HNF1B* gene. This mutation introduces an early translation stop codon and is predicted to result in a non-functional truncated protein that lacks the DNA binding and transactivation domains (Figure 6A). The *HNF1B*<sup>-/-</sup> iPSC lines underwent organoid formation in a similar time frame as the parental line and with equivalent efficiency (Figures S7A–S7D). Bright-field imaging of whole organoids showed that by day 14, *HNF1B*<sup>-/-</sup> organoids were slightly larger than controls (Figures 6B and 6C). Expression analysis by qPCR revealed little change in podocyte genes (*NPHS1*, *WT1*) and *GATA3* but a significant downregulation in markers of the proximal tubule (*LRP2*), thick ascending limb (*UMOD*, *SLC12A1*), *CDH1*, and *PAX2*, as well as the HNF1B transcriptional targets *HNF4A* and *PKHD1* (*UMOD* is also a direct target of HNF1B; Figure 6D). Consistent with these findings, immunostaining of day-14 organoids shows a loss of HNF1B protein (a pan-marker of tubules and collecting duct), LTL, and *SLC12A1* in *HNF1B*<sup>-/-</sup> organoids (Figures 6E–6J). A similar phenotype was seen as early as day 8 with loss of LTL and HNF1B but normal levels of *WT1*, *PAX2*, and *GATA3* (Figures S7E and S7F). Together, these findings indicate that disruption of *HNF1B* leads to a failure in the formation of the proximal tubule and thick ascending limb segments, much like that described in the mouse knockout (Heliot et al., 2013; Massa et al., 2013), with only podocytes and *GATA3*<sup>+</sup> distal nephron segments/presumptive collecting ducts forming in the *HNF1B*<sup>-/-</sup> organoids.

## DISCUSSION

Multiple approaches for differentiating pluripotent stem cells into kidney organoids have been reported (Yamaguchi

et al., 2016; Li et al., 2016; Brown et al., 2015; Takasato et al., 2015; Morizane et al., 2015; Freedman et al., 2015; Taguchi et al., 2014). In contrast to most of these methods, we developed an EB-based strategy that generates 3D aggregates of pluripotent stem cells that better mimic the structure of the developing embryo (Höpfl et al., 2004). Specifically, the EB environment is thought to be conducive to the formation of endogenous morphogenic gradients and fosters cell sorting and self-assembly. Such processes are less efficient in monolayer cultures and this may explain the lack of robustness of other methods (Serra et al., 2012). Not all of the EBs formed by our method give rise to kidney organoids, with smaller aggregates often failing to generate tubular tissue. This observation is in keeping with prior work with EBs in which the “quality” of terminal differentiation is dependent on EB size/cell number (Mohr et al., 2010; Meszana et al., 2008), presumably due to a minimal threshold of cells needed to mimic the developing embryo. The range in EB sizes generated by our approach is probably the result of differences in the sizes of the iPSC colony fragments, which itself is influenced by the starting confluence and the extent of mechanical dissociation. Because our approach is easily scalable, it is possible to generate a large number of EBs. As a result, size exclusion via sieving provides a rapid and labor-efficient way of enriching for organoids with optimal differentiation potential.

A key innovation of our method is the discovery that KOSR can replace more expensive supplements such as B27 used by Freedman et al. (2015) and FGF2/9 used in other protocols (Takasato et al., 2015; Morizane et al., 2015; Li et al., 2016; Taguchi et al., 2014). At this stage it is not clear how KOSR substitutes for the FGF signaling pathway, which acts by maintaining nephron progenitors in an undifferentiated state *in vivo* (Barak et al., 2012). KOSR and B27 both contain transferrin and insulin, and

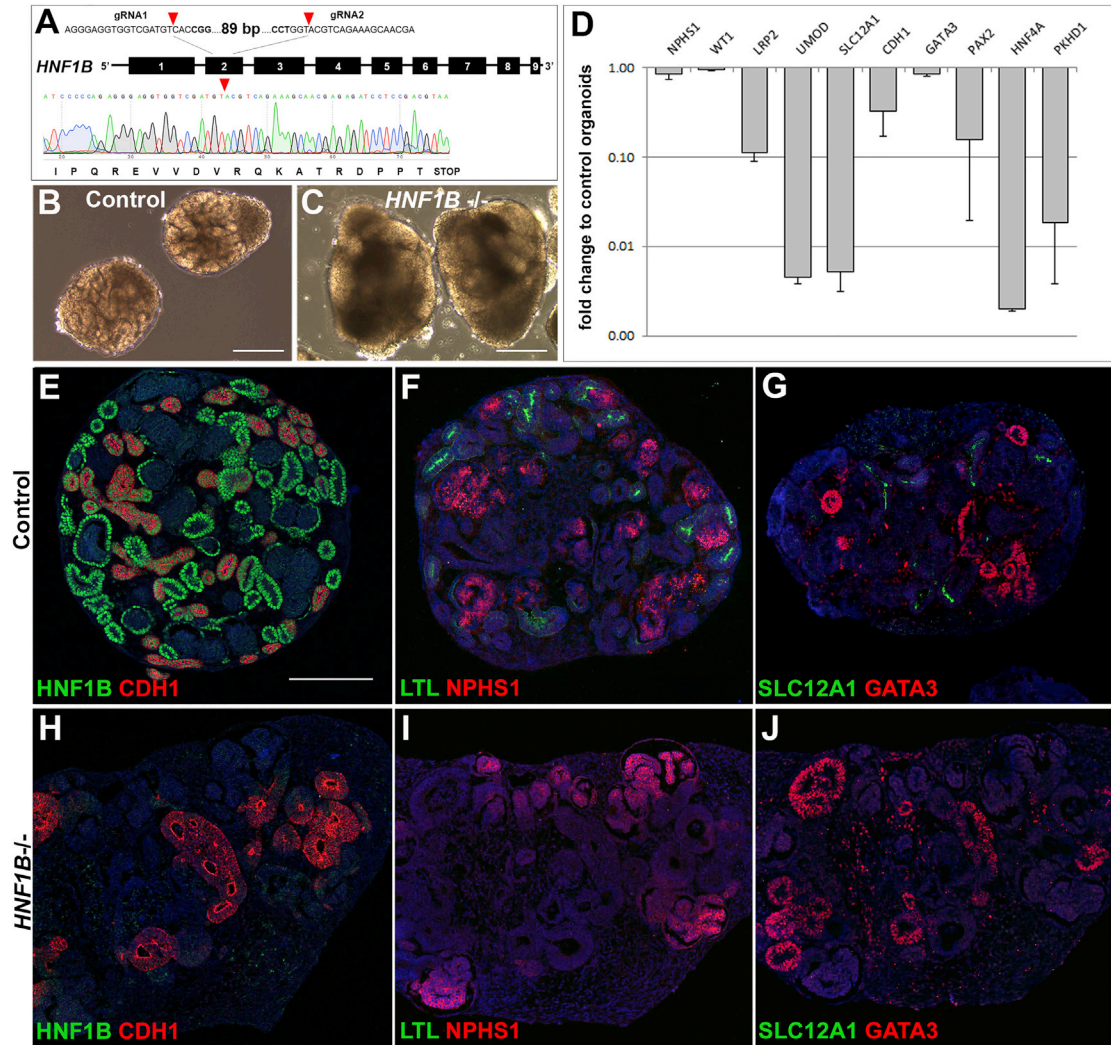


**Figure 6. Characterization of HNF1B<sup>-/-</sup> Organoids**

(A) Schematic overview of the CRISPR/Cas9-based strategy to disrupt the *HNF1B* gene. The deletion in exon 2 is marked with red arrowheads, and the Sanger sequencing chromatogram shows how the resulting frameshift causes a premature stop codon. (B and C) Bright-field images of control and *HNF1B*<sup>-/-</sup> organoids at day 14. (D) qPCR analysis of selected renal markers and known targets of HNF1B (*HNF4A*, *PKHD1*, *UMOD*) in day-14 *HNF1B*<sup>-/-</sup> kidney organoids compared with controls. Data are presented as means ± SD from technical triplicates. (E–J) Paraffin sections of control and *HNF1B*<sup>-/-</sup> kidney organoids at day 14 for HNF1B (green), LTL (proximal tubule, green), SLC12A1 (thick ascending limb, green), NPHS1 (podocytes, red), and CDH1 and GATA3 (distal tubule and collecting duct, red). n ≥ 3 sections per antibody combination. Nuclear counterstain: DAPI. Scale bars (B, C, and E–J), 200 μm.

these factors are essential for the serum-free culture of fetal kidney explants, where they act synergistically to support growth (Thesleff and Ekblom, 1984; Brewer et al., 1993; Garcia-Gonzalo and Belmonte, 2008; Brière et al., 1991). Whether insulin and transferrin are the key FGF-substituting components in KOSR and B27 remains to be determined. Regardless, our identification of KOSR as an inexpensive Stage II medium is a major advance since it

lowers the cost per assay, thereby enabling organoid generation at large scales. This breakthrough is a critical prerequisite for efforts to develop kidney organoids as a platform for nephrotoxicity testing and for future clinical applications such as cell replacement therapies (Morizane and Bonventre, 2017b).

With regard to technical complexity, our protocol differs from existing methods by being very simple with few



handling steps. For instance, the 3D culture method of [Morizane et al. \(2015\)](#), which produces organoids that are morphologically similar to ours, involves additional dissociation and centrifugation steps, as well as laborious growth in 96-well plates. Moreover, the most recent method by Taguchi's group requires separate induction of nephron and collecting duct progenitors followed by their co-culture ([Taguchi and Nishinakamura, 2017](#)). In our protocol, the EBs are formed in suspension, thus enabling them to be size-selected and transferred with ease to spinner flasks with minimal effort and time. Perhaps as a result of these fewer handling steps, we observe rapid tubule formation with structures visible by bright-field microscopy as early as day 8, in contrast to other methods that take between 12 and 21 days ([Chuah and Zink, 2017](#); [Kaminski et al., 2017](#)).

The organoids made from our protocol develop a well-defined proximal-distal segmentation pattern at day 14 that is comparable with other reports ([Takasato et al., 2015](#); [Morizane et al., 2015](#); [Freedman et al., 2015](#); [Taguchi et al., 2014](#); [Brown et al., 2015](#); [Li et al., 2016](#)). A direct comparison with fetal human kidney tissue suggests that our day-14 organoid nephrons correspond to the late capillary loop stage. We anticipated that longer culture times would improve the differentiation of our organoid nephrons. While this appears to be the case for podocytes, we found that the expression of tubule segment markers decreases after day 14 and that overlapping staining of LTL and CDH1 becomes more widespread. Based on observations in the mouse ([Cho et al., 1998](#)), it has been suggested that LTL<sup>+</sup>/CDH1<sup>+</sup> tubules represent mature proximal tubules ([Takasato et al., 2015](#)). However, in human fetal and adult kidneys we did not observe appreciable overlap with LTL and CDH1, except at a low level in descending limbs in the most mature of the fetal nephrons. While the LTL<sup>+</sup>/CDH1<sup>+</sup> tubules in the organoids may represent differentiation to a descending limb-like identity, given the reduced marker level and the dysmorphic appearance of some of the tubules at day 26, we favor the interpretation that it represents an aberrant state. In support of this, human distal tubule cells have a tendency to transdifferentiate into proximal tubule cells in culture ([Baer et al., 1999](#); [Van der Hauwaert et al., 2013](#)). This issue of cell identity is of particular importance to resolve, given that nephrotoxins such as cisplatin have been found to only induce injury in LTL<sup>+</sup>/CDH1<sup>+</sup> tubules and not LTL<sup>+</sup>-only tubules in kidney organoids ([Takasato et al., 2015](#)).

The decline in organoid "quality" after day 14 may be related to the fibrotic changes we observed at day 26. We found extensive proliferation of MEIS1/2/3<sup>+</sup> interstitial cells that co-label with ACTA2, a marker of pro-fibrotic myofibroblasts, and the deposition of collagen-rich extracel-

lular matrix. Renal fibrosis is the common endpoint of end-stage renal failure and is thought to result from a maladaptive wound-healing response ([Humphreys, 2018](#)). It is possible that culture beyond day 14 leads to tubular injury, perhaps in response to limitations in the mass transport of oxygen or nutrients into the organoid. While we sieve out large organoids with overt core apoptosis, the smaller organoids may still be undergoing sublethal levels of stress and releasing pro-fibrotic factors ([Maarouf et al., 2016](#)). If diffusion of oxygen/nutrients was responsible we might expect to see the fibrosis restricted to the core; however, it appears throughout the organoid even in peripheral locations. Therefore, there may be other inducers of the fibrosis such as intrinsic changes to the tubules related to aging or altered metabolism in culture. Proliferative changes in the growth of the tubules and interstitium also coincides with the fibrotic phenotype, with both populations dividing at day 14 whereas at day 26, growth is largely restricted to MEIS1/2/3<sup>+</sup>/ACTA2<sup>+</sup> cells. Large numbers of stromal cells are seen in kidney organoids reported by other methods, suggesting that this issue of interstitial expansion is a widespread problem ([Takasato et al., 2015](#); [Morizane and Bonventre, 2017a](#)). As the pathogenesis of renal fibrosis remains poorly understood and is complicated by the involvement of the immune system in animal models, kidney organoids may provide a useful tool to dissect the non-immune signals involved and for the screening of anti-fibrotic drugs.

To demonstrate the utility of our protocol to study human kidney development, we used gene editing in iPSCs to disrupt the *HNF1B* gene, which is implicated in congenital anomalies of the kidney and urinary tract in 10% of cases in humans ([Nakayama et al., 2010](#)). Kidney organoids made from *HNF1B*<sup>-/-</sup> iPSCs contained podocytes and GATA3<sup>+</sup> presumptive collecting ducts but lacked cells with either proximal or distal nephron identities. This phenotype closely resembles the rudimentary nephrons observed in *Hnf1b* conditionally deficient mice, where glomeruli are found connected to the collecting duct system via a short primitive tubule ([Heliot et al., 2013](#); [Massa et al., 2013](#)). Our phenocopy of this result validates the use of kidney organoids as a human-based system to study renal gene function. *Hnf1b*<sup>-/-</sup> mice (and individuals with heterozygous mutations in *HNF1B*) also develop renal cysts ([Desgrange et al., 2017](#)), but these were not observed in our *HNF1B*<sup>-/-</sup> kidney organoids even after several weeks in culture (data not shown). This is in contrast to recent work, wherein kidney organoids were used to recapitulate polycystic kidney disease ([Cruz et al., 2017](#); [Freedman et al., 2015](#)). Whether additional mutations or altered culture techniques are required to induce the formation of cystic collecting ducts in *HNF1B*<sup>-/-</sup> kidney organoids remains to be determined.



In summary, our new approach for generating kidney organoids is simple, rapid, scalable, and works robustly for a range of different pluripotent stem cell lines. Our method overcomes many of the drawbacks hampering existing protocols and provides the advance needed in order for kidney organoids to be effectively used for future applications such as drug testing and cell replacement therapies where there is a requirement to generate large amounts of tissue.

## EXPERIMENTAL PROCEDURES

### Fetal Human Tissue

Consented, de-identified human fetal tissue from elective terminations was collected following review of the study by the Institutional Review Board at Keck School of Medicine of the University of Southern California. See [Supplemental Information](#) for further information.

All experiments were performed with the three iPSC lines described below. For immunostaining, electron microscopy, and qPCR, data are representative of all three lines (unless stated otherwise). Individual stainings and measurements were performed at least in triplicate.

### iPSC Lines

All work was carried out with the approval of Human Participants Ethics Committees (UAHPEC 8712 and HDEC 17/NTA/204) and biosafety approval (GMO05). BJ RiPS (reprogrammed by RNA) was a gift from Dr. Chad Cowan ([Warren et al., 2010](#)). CRL1502 clone C32 (reprogrammed by episomal vectors) was developed in the Wolvetang laboratory ([Briggs et al., 2013](#)). The MANZ-2-2 line was generated in the Davidson laboratory (see [Supplemental Information](#)).

### Organoid Formation

Prior to EB formation, iPSCs were cultured on a 10-cm Geltrex-coated dish to 40%–50% confluence at which point discrete colonies have formed. Cells were washed twice with Dulbecco's PBS and incubated with 2 mL of 1 mg/mL dispase for 6 min at 37°C. Cells were washed three times with DBPS, scraped with a cell lifter, resuspended in BPEL plus 8  $\mu$ M CHIR99021, 3.3  $\mu$ M Y27632, and 1 mM  $\beta$ -mercaptoethanol, and evenly distributed into ultra-low 6-well attachment plates (Corning). BPEL medium was prepared as described in [Ng et al. \(2008\)](#) but with 0.1 $\times$  ITS-X as per [Orlova et al. \(2014\)](#). Half medium change was carried out on day 2 with BPEL supplemented with 8  $\mu$ M CHIR99021. On day 3, EBs were allowed to sediment in a 50-mL tube and washed twice in DMEM. EBs were returned to the ultra-low 6-well attachment plate and transferred to Stage II culture medium (DMEM, 15% KOSR [Thermo Fisher], 1% non-essential amino acids, 1% penicillin/streptomycin, 1% HEPES, 1% GlutaMAX, 0.05% poly(vinyl alcohol), 2.5  $\mu$ g/mL Plasmocin). Upon tubule formation (days 7–8), organoids were transferred into a 125-mL spinner flask (Corning) in 45 mL of Stage II medium, stirring at 90 rpm, with half medium change every 2 days. Alternatively, organoids were left in the ultra-low 6-well attachment plate and agitated using an orbital shaker ([Hubert et al., 2016](#)). No quantitative or qualitative differ-

ences in organoid number were observed when grown in either spinner flasks or 6-well plates. One milliliter of medium was determined to be the minimum volume for culturing of  $\sim$ 50 organoids. Therefore, the 6-well plate format is restricted to 900 organoids (with 3 mL of medium per well), whereas a 125-mL spinner flask can be scaled up to a maximum of 6,250 organoids.

### Size Filtration and Measurement

Organoids were passed through 200- and 500- $\mu$ m strainers (pluriStrainer). Whole organoid photos were acquired in bright field on an EVOS XL inverted microscope and analyzed using ImageJ. For efficiency, a random subset of each assay was photographed and counted for tubular versus non-tubular organoids at day 8. For size measurements a whole assay was analyzed.

### Reabsorption Assay

20  $\mu$ g/mL 10-kDa rhodamine-dextran was added to Stage II culture medium for 48 hr. Organoids were washed in Stage II medium for 5 hr before fixation in 4% paraformaldehyde, paraffin embedding, and sectioning.

### HNF1B Knockout

Guide RNA (gRNA) pairs targeted to introduce an 89-bp deletion in exon 2 of the *HNF1B* gene were designed using the RGEN, COSMID, and CCTop online tools ([Park et al., 2015](#); [Cradick et al., 2014](#); [Stemmer et al., 2015](#)). gRNAs were cloned into the pSpCas9(BB)-2A-GFP (Addgene 48138) construct, and knockout efficiencies for gRNA pairs were evaluated in HEK293 cells. Plasmids containing the gRNAs with highest knockout efficiency (gRNA1: 5'-AGG GAG GTG GTC GAT GTC ACC GG-3'; gRNA2: 5'-CCT GGT ACG TCA GAA AGC AAC GA-3') were introduced into the MANZ-2-2 iPSC line by reverse transfection using TransIT-LT1 (Mirus Bio). 48 hours after transfection, GFP-positive cells were isolated by fluorescence-activated cell sorting and 8,000 cells were plated on a 10-cm Geltrex-coated dish into pre-warmed mTeSR1 plus 5  $\mu$ M Y27632. Medium was changed daily using conditioned mTeSR1 without Y27632. Single colonies were manually picked when they had reached a suitable size ( $\sim$ 10 days post plating), clonally expanded, and screened for biallelic deletion clones using PCR primers flanking the deleted region ([Peters et al., 2013](#)). Homozygote deletions were verified by Sanger sequencing. Clones were expanded, karyotyped, and used for organoid assays. Control experiments were carried out with MANZ-2-2 iPSCs.

See [Supplemental Information](#) for additional experimental procedures.

## SUPPLEMENTAL INFORMATION

Supplemental Information includes Supplemental Experimental Procedures, seven figures, two tables, and one video and can be found with this article online at <https://doi.org/10.1016/j.stemcr.2018.06.018>.

## AUTHOR CONTRIBUTIONS

A.P., T.M.H., and A.J.D. conceptualized the study; A.P. and V.S. designed the experiments; A.P. established the protocol; A.P. and V.S.



conducted organoid culture, processing, and analysis; V.S. generated the *HNF1B* knockout; T.T. analyzed human fetal kidney tissue; A.P., J.A.H., J.-H.S., B.S., and T.M.H. generated the MANZ-2-2 iPSC line; E.J.W. generated the C32 iPSC line; A.P.M. and T.M.H. co-supervised the study; A.P., V.S., and A.J.D. wrote the manuscript; A.J.D. supervised the study; V.S., A.P.M., and A.J.D. acquired funding.

## ACKNOWLEDGMENTS

We thank Adrian Turner, Jacqui Ross, and Satya Amirapu for help with histology and microscopy, Paula Lewis for critical reading of the manuscript, and Peter Shepherd for providing resources to facilitate the project. Work in A.J.D.'s laboratory was supported by the Health Research Council of New Zealand (17/425), Auckland Medical Research Foundation (1116018), Cystinosis Research Foundation USA, Cystinosis Research Ireland Foundation (MRCG-2014-8) Maurice Wilkins Center, and Valrae Collins Philanthropic support for A.P. Work in A.P.M.'s laboratory was supported by the NIH (DK054364) and California Institute of Regenerative Medicine (LA1-06536).

Received: December 15, 2017

Revised: June 21, 2018

Accepted: June 22, 2018

Published: July 19, 2018

## REFERENCES

- Baer, P.C., Tunn, U.W., Nunez, G., Scherberich, J.E., and Geiger, H. (1999). Transdifferentiation of distal but not proximal tubular epithelial cells from human kidney in culture. *Exp. Nephrol.* *7*, 306–313.
- Barak, H., Huh, S.H., Chen, S., Jeanpierre, C., Martinovic, J., Parisot, M., Bole-Feysot, C., Nitschke, P., Salomon, R., Antignac, C., et al. (2012). FGF9 and FGF20 maintain the stemness of nephron progenitors in mice and man. *Dev. Cell* *22*, 1191–1207.
- Brewer, G.J., Torricelli, J.R., Evege, E.K., and Price, P.J. (1993). Optimized survival of hippocampal neurons in B27-supplemented Neurobasal, a new serum-free medium combination. *J. Neurosci. Res.* *35*, 567–576.
- Brière, N., Chailler, P., and Ferrari, J. (1991). Insulin and transferrin restore important cellular functions of human fetal kidney in serum-free organ culture. *Biochem. Cell Biol.* *69*, 256–262.
- Briggs, J.A., Sun, J., Shepherd, J., Ovchinnikov, D.A., Chung, T., Nayler, S.P., Kao, L., Morrow, C.A., Thakar, N.Y., Soo, S., et al. (2013). Integration-free induced pluripotent stem cells model genetic and neural developmental features of down syndrome etiology. *Stem Cells* *31*, 467–478.
- Brown, A.C., Muthukrishnan, S.D., and Oxburgh, L. (2015). A synthetic niche for nephron progenitor cells. *Dev. Cell* *34*, 229–241.
- Cho, E.A., Patterson, L.T., Brookhiser, W.T., Mah, S., Kintner, C., and Dressler, G.R. (1998). Differential expression and function of cadherin-6 during renal epithelium development. *Development* *125*, 803–812.
- Christensen, E.I., Nielsen, S., Moestrup, S.K., Borre, C., Maunsbach, A.B., de Heer, E., Ronco, P., Hammond, T.G., and Verroust, P. (1995). Segmental distribution of the endocytosis receptor gp330 in renal proximal tubules. *Eur. J. Cell Biol.* *66*, 349.
- Chuah, J.K.C., and Zink, D. (2017). Stem cell-derived kidney cells and organoids: recent breakthroughs and emerging applications. *Biotechnol. Adv.* *35*, 150–167.
- Clissold, R.L., Hamilton, A.J., Hattersley, A.T., Ellard, S., and Bingham, C. (2015). HNF1B-associated renal and extra-renal disease—an expanding clinical spectrum. *Nat. Rev. Nephrol.* *11*, 102–112.
- Cradick, T.J., Qiu, P., Lee, C.M., Fine, E.J., and Bao, G. (2014). COSMID: a web-based tool for identifying and validating CRISPR/Cas off-target sites. *Mol. Ther. Nucleic Acids* *3*, e214.
- Cruz, N.M., Song, X., Czerniecki, S.M., Gulieva, R.E., Churchill, A., Kim, Y.K., Winston, K., Tran, L.M., Diaz, M., Fu, H., et al. (2017). Organoid cystogenesis reveals a critical role of microenvironment in human polycystic kidney disease. *Nat. Mater.* *16*, 1112.
- Desgrange, A., Heliot, C., Skovorodkin, I., Akram, S.U., Heikkila, J., Ronkainen, V.P., Miinalainen, I., Vainio, S.J., and Cereghini, S. (2017). HNF1B controls epithelial organization and cell polarity during ureteric bud branching and collecting duct morphogenesis. *Development* *144*, 4704–4719.
- Dressler, G.R., and Woolf, A.S. (1999). Pax2 in development and renal disease. *Int. J. Dev. Biol.* *43*, 463.
- Freedman, B.S., Brooks, C.R., Lam, A.Q., Fu, H., Morizane, R., Agrawal, V., Saad, A.F., Li, M.K., Hughes, M.R., Werff, R.V., et al. (2015). Modelling kidney disease with CRISPR-mutant kidney organoids derived from human pluripotent epiblast spheroids. *Nat. Commun.* *6*, 8715.
- Garcia-Gonzalo, F.R., and Belmonte, J.C.I. (2008). Albumin-associated lipids regulate human embryonic stem cell self-renewal. *PLoS One* *3*, e1384.
- Heliot, C., Desgrange, A., Buisson, I., Prunskaitė-Hyyryläinen, R., Shan, J., Vainio, S., Umbhauer, M., and Cereghini, S. (2013). HNF1B controls proximal-intermediate nephron segment identity in vertebrates by regulating Notch signalling components and *Irx1/2*. *Development* *140*, 873–885.
- Höpfl, G., Gassmann, M., and Desbaillets, I. (2004). Differentiating embryonic stem cells into embryoid bodies. *Methods Mol. Biol.* *254*, 79–98.
- Hubert, C.G., Rivera, M., Spangler, L.C., Wu, Q., Mack, S.C., Prager, B.C., Couce, M., McLendon, R.E., Sloan, A.E., and Rich, J.N. (2016). A Three-dimensional organoid culture system derived from human glioblastomas recapitulates the hypoxic gradients and cancer stem cell heterogeneity of tumors found in vivo. *Cancer Res.* *76*, 2465–2477.
- Humphreys, B.D. (2018). Mechanisms of renal fibrosis. *Annu. Rev. Physiol.* *80*, 309.
- Kaminski, M.M., Tomic, J., Pichler, R., Arnold, S.J., and Lienkamp, S.S. (2017). Engineering kidney cells: reprogramming and directed differentiation to renal tissues. *Cell Tissue Res.* *369*, 185.
- Kirk, A., Campbell, S., Bass, P., Mason, J., and Collins, J. (2010). Differential expression of claudin tight junction proteins in the human cortical nephron. *Nephrol. Dial. Transplant.* *25*, 2107–2119.
- Kumar, R., Schaefer, J., Grande, J.P., and Roche, P.C. (1994). Immunolocalization of calcitriol receptor, 24-hydroxylase



- cytochrome P-450, and calbindin D28k in human kidney. *Am. J. Physiol.* **266**, 477.
- Labastie, M.C., Catala, M., Gregoire, J.M., and Peault, B. (1995). The GATA-3 gene is expressed during human kidney embryogenesis. *Kidney Int.* **47**, 1597–1603.
- Lam, A.Q., Freedman, B.S., Morizane, R., Lerou, P.H., Valerius, M.T., and Bonventre, J.V. (2014). Rapid and efficient differentiation of human pluripotent stem cells into intermediate mesoderm that forms tubules expressing kidney proximal tubular markers. *J. Am. Soc. Nephrol.* **25**, 1211–1225.
- Lancaster, M.A., and Knoblich, J.A. (2014). Organogenesis in a dish: modeling development and disease using organoid technologies. *Science* **345**, 1247125.
- Li, Z., Araoka, T., Wu, J., Liao, H., Li, M., Lazo, M., Zhou, B., Sui, Y., Wu, M., Tamura, I., et al. (2016). 3D culture supports long-term expansion of mouse and human nephrogenic progenitors. *Cell Stem Cell* **19**, 516–529.
- Lindstrom, N.O., McMahon, J.A., Guo, J., Tran, T., Guo, Q., Rutledge, E., Parvez, R.K., Saribekyan, G., Schuler, R.E., Liao, C., et al. (2018a). Conserved and divergent features of human and mouse kidney organogenesis. *J. Am. Soc. Nephrol.* **29**, 785–805.
- Lindstrom, N.O., Tran, T., Guo, J., Rutledge, E., Parvez, R.K., Thornton, M.E., Grubbs, B., McMahon, J.A., and McMahon, A.P. (2018b). Conserved and divergent molecular and anatomic features of human and mouse nephron patterning. *J. Am. Soc. Nephrol.* **29**, 825–840.
- Maarouf, O.H., Aravamudhan, A., Rangarajan, D., Kusaba, T., Zhang, V., Welborn, J., Gauvin, D., Hou, X., Kramann, R., and Humphreys, B.D. (2016). Paracrine Wnt1 drives interstitial fibrosis without inflammation by tubulointerstitial cross-talk. *J. Am. Soc. Nephrol.* **27**, 781–790.
- Mae, S., Shono, A., Shiota, F., Yasuno, T., Kajiwarra, M., Gotoda-Nishimura, N., Arai, S., Sato-Otubo, A., Toyoda, T., Takahashi, K., et al. (2013). Monitoring and robust induction of nephrogenic intermediate mesoderm from human pluripotent stem cells. *Nat. Commun.* **4**, 1367.
- Mantilla, J.G., Antic, T., and Tretiakova, M. (2017). GATA3 as a valuable marker to distinguish clear cell papillary renal cell carcinomas from morphologic mimics. *Hum. Pathol.* **66**, 152.
- Martin, Y., and Vermette, P. (2005). Bioreactors for tissue mass culture: design, characterization, and recent advances. *Biomaterials* **26**, 7481–7503.
- Massa, F., Garbay, S., Bouvier, R., Sugitani, Y., Noda, T., Gubler, M.C., Heidet, L., Pontoglio, M., and Fischer, E. (2013). Hepatocyte nuclear factor 1beta controls nephron tubular development. *Development* **140**, 886–896.
- McMahon, A.P. (2016). Development of the mammalian kidney. *Curr. Top. Dev. Biol.* **117**, 31.
- Messana, J.M., Hwang, N.S., Coburn, J., Elisseff, J.H., and Zhang, Z. (2008). Size of the embryoid body influences chondrogenesis of mouse embryonic stem cells. *J. Tissue Eng. Regen. Med.* **2**, 499–506.
- Mohr, J.C., Zhang, J., Azarin, S.M., Soerens, A.G., de Pablo, J.J., Thomson, J.A., Lyons, G.E., Palecek, S.P., and Kamp, T.J. (2010). The microwell control of embryoid body size in order to regulate cardiac differentiation of human embryonic stem cells. *Biomaterials* **31**, 1885–1893.
- Morizane, R., and Bonventre, J.V. (2017a). Generation of nephron progenitor cells and kidney organoids from human pluripotent stem cells. *Nat. Protoc.* **12**, 195–207.
- Morizane, R., and Bonventre, J.V. (2017b). Kidney organoids: a translational journey. *Trends Mol. Med.* **23**, 246–263.
- Morizane, R., Lam, A.Q., Freedman, B.S., Kishi, S., Valerius, M.T., and Bonventre, J.V. (2015). Nephron organoids derived from human pluripotent stem cells model kidney development and injury. *Nat. Biotechnol.* **33**, 1193–1200.
- Nakayama, M., Nozu, K., Goto, Y., Kamei, K., Ito, S., Sato, H., Emi, M., Nakanishi, K., Tsuchiya, S., and Iijima, K. (2010). HNF1B alterations associated with congenital anomalies of the kidney and urinary tract. *Pediatr. Nephrol.* **25**, 1073–1079.
- Naylor, R.W., Przepiorski, A., Ren, Q., Yu, J., and Davidson, A.J. (2013). HNF1 $\beta$  is essential for nephron segmentation during nephrogenesis. *J. Am. Soc. Nephrol.* **24**, 77–87.
- Ng, E.S., Davis, R., Elefanty, A.G., and Stanley, E.G. (2008). A protocol describing the use of a recombinant protein-based, animal product-free medium (APEL) for human embryonic stem cell differentiation as spin embryoid bodies. *Nat. Protoc.* **3**, 768–776.
- Orlova, V.V., Van Den Hil, F.E., Francijna, E., Petrus-reurer, S., Drabsch, Y., Dijke, P.T., and Mummery, C.L. (2014). Generation, expansion and functional analysis of endothelial cells and pericytes derived from human pluripotent stem cells. *Nat. Protoc.* **9**, 1514–1531.
- Pagliuca, F.W., Millman, J.R., Gurtler, M., Segel, M., Van Dervort, A., Ryu, J.H., Peterson, Q.P., Greiner, D., and Melton, D.A. (2014). Generation of functional human pancreatic-beta cells *in vitro*. *Cell* **159**, 428–439.
- Park, J., Bae, S., and Kim, J. (2015). Cas-Designer: a web-based tool for choice of CRISPR-Cas9 target sites. *Bioinformatics* **31**, 4014.
- Peters, D.T., Cowan, C.A., and Musunuru, K. (2013). Genome editing in human pluripotent stem cells. In *StemBook*, The Stem Cell Research Community, ed. (Harvard Stem Cell Institute).
- Serra, M., Brito, C., Correia, C., and Alves, P.M. (2012). Process engineering of human pluripotent stem cells for clinical application. *Trends Biotechnol.* **30**, 350.
- Stemmer, M., Thumberger, T., Del Sol Keyer, M., Wittbrodt, J., and Mateo, J.L. (2015). CCTop: an intuitive, flexible and reliable CRISPR/Cas9 target prediction tool. *PLoS One* **10**, e0124633.
- Taguchi, A., and Nishinakamura, R. (2017). Higher-order kidney organogenesis from pluripotent stem cells. *Cell Stem Cell* **21**, 730–746.e6.
- Taguchi, A., Kaku, Y., Ohmori, T., Sharmin, S., Ogawa, M., Sasaki, H., and Nishinakamura, R. (2014). Redefining the *in vivo* origin of metanephric nephron progenitors enables generation of complex kidney structures from pluripotent stem cells. *Cell Stem Cell* **14**, 53–67.
- Takasato, M., Er, P.X., Becroft, M., Vanslambrouck, J.M., Stanley, E.G., Elefanty, A.G., and Little, M.H. (2014). Directing human embryonic stem cell differentiation towards a renal lineage generates a self-organizing kidney. *Nat. Cell Biol.* **16**, 118–126.



- Takasato, M., Er, P.X., Chiu, H.S., Maier, B., Baillie, G.J., Ferguson, C., Parton, R.G., Wolvetang, E.J., Roost, M.S., Chuva de Sousa Lopes, S.M., et al. (2015). Kidney organoids from human iPS cells contain multiple lineages and model human nephrogenesis. *Nature* 526, 564–568.
- Takasato, M., and Little, M.H. (2016). A strategy for generating kidney organoids: recapitulating the development in human pluripotent stem cells. *Dev. Biol.* 420, 210–220.
- Thesleff, I., and Ekblom, P. (1984). Role of transferrin in branching morphogenesis, growth and differentiation of the embryonic kidney. *J. Embryol. Exp. Morphol.* 82, 147.
- Van der Hauwaert, C., Savary, G., Gnemmi, V., Glowacki, F., Pottier, N., Bouillez, A., Maboudou, P., Zini, L., Leroy, X., Cauffiez, C., et al. (2013). Isolation and characterization of a primary proximal tubular epithelial cell model from human kidney by CD10/CD13 double labeling. *PLoS One* 8, e66750.
- Warren, L., Manos, P.D., Ahfeldt, T., Loh, Y.H., Li, H., Lau, F., Ebina, W., Mandal, P.K., Smith, Z.D., Meissner, A., et al. (2010). Highly efficient reprogramming to pluripotency and directed differentiation of human cells with synthetic modified mRNA. *Cell Stem Cell* 7, 618–630.
- Winkle, A.P., Gates, I.D., and Kallos, M.S. (2012). Mass transfer limitations in embryoid bodies during human embryonic stem cell differentiation. *Cells Tissues Organs* 196, 34–47.
- Yamaguchi, S., Morizane, R., Homma, K., Monkawa, T., Suzuki, S., Fujii, S., Koda, M., Hiratsuka, K., Yamashita, M., Yoshida, T., et al. (2016). Generation of kidney tubular organoids from human pluripotent stem cells. *Sci. Rep.* 6, 38353.